

UC Davis

UC Davis Previously Published Works

Title

Physiological electric fields induce directional migration of mammalian cranial neural crest cells

Permalink

<https://escholarship.org/uc/item/7z9505tp>

Authors

Mehta, Abijeet Singh

Ha, Pin

Zhu, Kan

et al.

Publication Date

2021-03-01

DOI

10.1016/j.ydbio.2020.12.011

Peer reviewed

1 **Physiological electric fields induce directional migration of**
2 **mammalian cranial neural crest cells**

3 Abijeet Singh Mehta^{1,2,#}, Pin Ha^{3,#}, Kan Zhu^{1,2,#}, ShiYu Li^{1,2}, Kang Ting³, Chia Soo⁴, Xinli
4 Zhang^{3¶}, Min Zhao^{1,2¶}

- 5 1. Department of Ophthalmology & Vision Science, Institute for Regenerative Cures,
6 Center for Neuroscience, University of California at Davis, School of Medicine, Suite
7 1630, Room 1617, 2921 Stockton Blvd., Sacramento, CA, 95817, USA.
8 2. Department of Dermatology, University of California, Davis, CA, USA.
9 3. Section of Orthodontics, Division of Growth and Development, School of Dentistry,
10 University of California, Los Angeles, CA, USA.
11 4. Division of Plastic and Reconstructive Surgery and Department of Orthopaedic Surgery
12 and the Orthopaedic Hospital Research Center, University of California, Los Angeles,
13 CA 90095, USA

14
15
16 # contributed equally

17 ¶ corresponding authors

18
19 MZ: minzhao@ucdavis.edu

20 XZ: xzhang@dentistry.ucla.edu
21
22
23
24
25

26 word number of the main text: 2937

27 number of figures: 4
28

1 **ABSTRACT**

2 During neurulation, cranial neural crest cells (CNCCs) migrate long distances from the
3 neural tube to their terminal site of differentiation. The pathway traveled by the CNCCs
4 defines the blueprint for craniofacial construction, abnormalities of which contribute to
5 three-quarters of human birth defects. Biophysical cues like naturally occurring electric
6 fields (EFs) have been proposed to be one of the guiding mechanisms for CNCC
7 migration from the neural tube to identified position in the branchial arches. Such
8 endogenous EFs can be mimicked by applied EFs of physiological strength that has been
9 reported to guide the migration of amphibian and avian neural crest cells (NCCs), namely
10 galvanotaxis or electrotaxis. However, the behavior of mammalian NCCs in external EFs
11 has not been reported. We show here that mammalian CNCCs migrate towards the
12 anode in direct current (dc) EFs. Reversal of the field polarity reverses the directedness.
13 The response threshold was below 30mV/mm and the migration directedness and
14 displacement speed increased with increase of field strength. Both CNCC line (O9-1) and
15 primary mouse CNCCs show similar galvanotaxis behavior. Our results demonstrate for
16 the first time that the mammalian CNCCs respond to physiological EFs by robust
17 directional migration towards the anode in a voltage-dependent manner.

18

19 **Key words**

20 Galvanotaxis; Electrotaxis; Cranial neural Crest Cells; O9-1; Electric fields; Directional
21 cell migrations; Mouse.

22

1 INTRODUCTION

2 Neural crest cells (NCCs), a “fourth germ layer”, is innovation that developed in
3 vertebrates as they evolved from protochordates (Hall, 2000; Hu et al., 2014). It facilitated
4 the generation of novel vertebrate head structures that contributed to chordate diversity
5 and adaptation to most niches of the planet. Originally identified by William His in 1868,
6 NCCs originate from the dorsal half of the developing neural tube (Ruhrberg and
7 Schwarz, 2010). During neurulation, dorsal neuroepithelial cells undergo epithelial-to-
8 mesenchymal transition (EMT), followed by a rostrocaudal emigrational wave of NCCs to
9 the terminal site of differentiation (Baker and Bronner-Fraser, 1997; Litsiou et al., 2005).
10 Based on their axial position of origin, and differentiating lineage, NCCs can be
11 categorized as cranial, sacral, vagal, or trunk (Barlow et al., 2012; Hall, 2000; Walker and
12 Trainor, 2006). Cranial neural crest cells (CNCCs) can be considered as multipotent
13 progenitors that can differentiate into most of the cartilage and bone of the skull, face,
14 and pharyngeal skeleton (Crane and Trainor, 2006). They can migrate long distances,
15 from the neural tube to the branchial arches, with the aim of sculpting a scaffold for
16 vertebrate craniofacial development (Trainor, 2010; Trainor et al., 2002). Three-quarters
17 of human birth defects involve craniofacial abnormalities. Annual treatment cost for
18 children born with cleft lip and/ or cleft palate alone is US\$697 million (Cordero et al.,
19 2011; Trainor, 2010). This highlights the importance of studying how CNCCs establish
20 stereotypical directional migratory behavior and acquire positional identity to architect the
21 destined structure (Craniofacial) (Mehta and Singh, 2019; Minoux and Rijli, 2010).

22 CNCCs detect various micro environmental cues that guide their long distance
23 migration (Epperlein et al., 2007; Gilbert et al., 2007; Golding et al., 2000; Gov, 2007;

1 Kulesa and Fraser, 1998; Reyes et al., 2010; Wynn et al., 2013). Significant progress has
2 been made in underpinning the molecular mechanisms and gene regulatory networks that
3 are crucial for targeted CNCC migration (Litsiou et al., 2005; Minoux and Rijli, 2010). In
4 recent years, considerable progress has also been made to identify environmental cues
5 (chemoattractant and mechanical signals) that are involved in long distance migration of
6 CNCCs (Abzhanov et al., 2006; Bajanca et al., 2019; Barriga et al., 2018; Marcucio et al.,
7 2005; Shellard and Mayor, 2019; Szabó et al., 2019; Walheim et al., 2012).

8 Endogenous EFs are present during neurulation (Metcalf et al., 1994; Shi and
9 Borgens, 1995). During amphibian embryogenesis electric current is driven out of the
10 lateral margins of the neural tube, and out of the blastopore, and returns inward at the
11 neural groove and at the lateral skin, creating an EF gradient of 27 ± 4 mV/mm along the
12 rostral-caudal axis, which changes temporally during neurulation (Hotary and Robinson,
13 1994; Metcalf et al., 1994; Shi and Borgens, 1995). Manipulating these electric fields
14 (EFs) caused neurocristopathies, e.g. retarded eye development and reduced head
15 formation (Hotary and Robinson, 1994), suggesting contributing role of the EFs.

16 Applied EFs of physiological strength can guide direction cell migration, suggesting
17 involvement of EFs in directed cell migration (Chang and Minc, 2014; Levin et al., 2017;
18 Levin et al., 2019; Mathews and Levin, 2018). Different putative sensors have been
19 suggested that can determine cell directedness (Allen et al., 2013; Forrester et al., 2007;
20 Kennard and Theriot, 2020; Zhao et al., 2020). In culture, avian and amphibian NCCs
21 respond to applied EFs by directional migration (galvanotaxis / electrotaxis) towards the
22 cathode (Cooper and Keller, 1984; Gruler and Nuccitelli, 1991; Nuccitelli and Smart,
23 1989). It is however not known whether mammalian NCCs respond to EFs, and what is

1 their preferred directedness. We report here that a well-characterized cranial NCC line,
2 'O9-1' showed robust directional migration toward the anode in applied EFs, and primary
3 cultures of NCCs of the same cranial lineage had the same anodal galvanotaxis.

1 MATERIALS AND METHODS

2 Cell Culture

3 O9-1 mouse CNCC line is an extended culture of primary CNCCs isolated from E8.5
4 mouse embryo, which express NCC markers, and can differentiate into osteoblasts,
5 chondrocytes, smooth muscle cells, and glial cells (Ishii et al., 2012). The O9-1 cell line
6 (Sigma Millipore, Cat# SCC049) was cultured in cell culture flasks pre-coated with 1:50
7 diluted Matrigel™ (Fisher, Cat# CB-40234) at room temperature for 1 hour; then cells
8 were grown in complete ES cell medium with 15% FBS and LIF (Sigma Millipore, Cat#
9 ES-101-B) + 25 ng/ml recombinant human bFGF (Sigma Millipore, Cat# GF003) at 37 °C,
10 5% CO₂. Primary mouse CNCCs were isolated from the frontal and nasal bones of the
11 cranial vault of neonatal wildtype C57BL/6J mouse, following the established protocol
12 (Chen et al., 2019; Wong and Cohn, 1975; Zhang et al., 2002). They were cultured in
13 growth medium containing high glucose DMEM + 10% heat-inactivated fetal bovine
14 serum (FBS) + 100 U/ml penicillin/streptomycin (P/S) at 37 °C, 5% CO₂. Passage 3-5 of
15 primary cells were used. The animals use was approved by the UCLA IACUC committee.

16 Real-time quantitative polymerase chain reaction (RT- qPCR)

17 Real-time PCR was performed using the QuantStudio™ 3 real-time PCR System
18 instrument (Applied Biosystems, Foster City, CA, USA) as described previously (Ishii et
19 al., 2012; James et al., 2015; Mehta et al., 2019; Mehta and Singh, 2017). A set of
20 representative genes of NCCs were selected to define the cells in this study (Ishii et al.,
21 2012; Szabo and Mayor, 2018; Trainor, 2005) (**Table 1**). All data are representative of
22 three experimental set of cells with PCR triplicates and are presented as the fold change.

1

Table 1

Primer	Sequence (Forward)	Sequence (Reverse)
GAPDH	5'-ATTCAACGGCACAGTCAAGG-3'	5'-GATGTTAGTGGGGTCTCGCTC-3'
Snail1	5'-CTTGTGTCTGCACGACCTGT-3'	5'-CTTCACATCCGAGTGGGTTT-3'
Twist1	5'-GGAGGATGGAGGGGGCCTGG-3'	5'-TGTGCCCCACGCCCTGATTC-3'
Nestin	5'-AATGGGAGGATGGAGAATGGAC-3'	5'-TAGACAGGCAGGGCTAGCAAG-3'
CD44	5'-GTGGCACACAGCTTGGGGA-3'	5'-TCAGAGCCAGTGCCAGGAGAGAT-3'
Sca-1	5'-CTCTGAGGATGGACACTTCT-3'	5'-GGTCTGCAGGAGGACTGAGC-3'

2 Alkaline phosphatase (ALP) and mineralization assays

3 Osteogenic differentiation of CNCCs is assayed using the leukocytes ALP staining Kit
 4 (Sigma-Aldrich, Cat# 86R-1KT) and Alizarin Red (AR) staining with 2% Alizarin Red
 5 stains (Lifeline, Cat# CM-0058) (Chen et al., 2019). On Day-7 of initiation of
 6 differentiation, the cells were fixed in 4% paraformaldehyde and incubated with a mixture
 7 of Naphthol AS-BI alkaline solution and FRV-alkaline solution. Areas that stained pink or
 8 light purple were designated as positive. For AR staining, on Day-21, cells were fixed in
 9 4% paraformaldehyde and incubated with 2% Alizarin Red stains. Calcification nodules
 10 were stained bright red after thorough wash with water.

11 Galvanotaxis assay and time lapse imaging

12 Galvanotaxis experiments were done as described previously (Cooper and Keller, 1984;
 13 Song et al., 2007). CNCCs were loaded into the electrotactic chamber (pre-coated with
 14 1:50 diluted Matrigel™) with a density of ~100 cells per square millimeter. The cells were
 15 incubated for 4 hours at 37°C with air containing 5% CO₂ to allow attachment. Agar/saline
 16 (100% Steinberg's solution gelled with 1% agar) bridges were placed into the chamber
 17 channels and connected to wells containing 100% Steinberg's solution and silver-silver
 18 chloride electrodes. Time-lapse images of 5-min intervals of cells were acquired using an
 19 inverted microscope (Carl Zeiss, Oberkochen, Germany).

1 ImageJ (National Institutes of Health) software was used to analyze cell migration
2 as described (Song et al., 2007). 'Directedness' is the quantitative measurement of how
3 directionally cells migrated in response to an EF. The directedness was assessed as
4 cosine θ , in which θ was the angle between EF direction and a straight line that connects
5 the start and end positions of a cell. A cell moving directly to the cathode or the anode
6 would have a directedness value of 1 or -1 , respectively. Migration distance (in μm) is
7 calculated as (1) accumulated distance, which is the full trajectory distance traveled by
8 the cell, and (2) Euclidean distance, which is the straight-line distance between the
9 starting and final positions of a cell. Displacement speed (in $\mu\text{m}/\text{min}$) is the Euclidean
10 distance over time.

11 **Statistics**

12 Statistical analysis was performed using unpaired, two tailed student *t*-test. Data are
13 expressed as mean \pm SEM. *P*-value less than 0.05 was considered statistically significant.

1 RESULTS

2 Mammalian CNCCs show anodal galvanotaxis

3 We first determined the migratory response of mammalian CNCCs O9-1 line to applied
4 EFs. In control condition without EFs, cells migrated actively in random direction (**Fig. 1,**
5 **A,B** and **Movie 1**). When a direct current (dc) EF was applied, the cells showed robust
6 directional migration towards the anode (**Fig. 1, C,D** and **Movie 2**).

7 This noteworthy impact on the migration directedness of O9-1 cells, imposed by a
8 dcEF, is further illustrated by reversing the field polarity. We reversed the EF polarity after
9 CNCCs have been exposed to an EF and migrated for 2h in one direction, then reversed
10 the field direction 180°. In the first 2h, as expected cells migrated towards the anode (left)
11 (**Fig 1. E,F** and **Movie 3**). Within 5-10 minutes following the polarity reversal, cells started
12 migrating towards the new anode (right) (**Fig1. E,G** and **Movie 3**). The migration
13 trajectories of the individual cells show the directional change upon reversal of the field
14 polarity (**Fig 1. F,G**). O9-1 cells in culture thus showed anodal galvanotaxis.

15 Voltage dependent responses of mammalian CNCCs

16 To determine the threshold voltage for galvanotaxis of O9-1 cells, we applied EFs of
17 different strength. We found that at the low field strength of 15 mV/mm, CNCCs did not
18 show statistically significant change in migration direction (**Fig 2. A,G** and **Movie 4**).
19 However, in a field with strengths of 30 mV/mm and greater, CNCCs show statistically
20 significant directional migration towards the anode (**Fig 2. B-G** and **Movie 4**), suggesting
21 that the threshold for O9-1 cell galvanotaxis is between 15mV/mm – 30mV/mm (**Fig 2.**

1 **B,G).**

2 Displacement speed of O9-1 cells show progression with the increase in EF
3 strengths (**Fig 2. H**). The displacement speed in the absence of EF is 0.45 ± 0.04
4 ($\mu\text{m}/\text{mm}$), which significantly increased to 0.829 ± 0.08 in an EF of 30 mV/mm and
5 continues to increase with the increase in field strength. The threshold for increased
6 displacement speed is likely between 15-30mV/mm.

7 **Galvanotaxis of primary cultures of CNCCs**

8 Next, to rule out any cell line specific response, we used primary cultures of CNCCs to
9 test galvanotaxis of the same cranial lineage. The primary cells were from the frontal and
10 nasal bones of neonatal wildtype (C57BL/6J) mouse cranial vault (**Fig 3. A**). This region
11 in mouse is derived only from CNCCs (Chen et al., 2020; Jiang et al., 2002). The primary
12 cells were validated for their CNCC properties by performing RT-qPCR of representative
13 markers (*Snail1*, *Twist1*, *Nestin*, *CD44* and *Sca-1*) (Ishii et al., 2012; Szabo and Mayor,
14 2018; Trainor, 2005) (**Fig 3. B**). Expression of those markers were confirmed in the O9-1
15 cells as well, which were used to normalize expression levels in the primary cells. Also,
16 differentiation potentials of both O9-1 and primary CNCCs were tested for osteogenesis
17 (**Fig 3. C**). Potency of osteogenesis distinguishes CNCCs from other NCC populations
18 (Le Douarin and Kalchheim, 1999; Noden, 1988; Santagati and Rijli, 2003; Szabo and
19 Mayor, 2018). We placed cells in osteogenic conditions and performed ALP staining and
20 AR staining at different time points (Day-7 and Day-21 following differentiation induction).
21 Both types of cells achieved positive ALP activity, and mineralization stained by AR (**Fig**
22 **3. C**).

1 We recorded voltage dependent response of primary CNCCs. Similar to cell lines
2 (O9-1), directed migration of primary CNCCs also improved with increasing field strength
3 **(Fig 3. D-I and Movie 5,6)**. Effect on migration directedness became significant at
4 100mV/mm, and further at 200mV/mm. The effect on displacement speed however,
5 started to show significance even at much lower field strength of 15mV/mm, which was
6 further increased at 100-200mV/mm (4-5 times faster than that of no EF control) **(Fig 3.**
7 **I)**.

8 **Culture density of CNCCs did not affect galvanotaxis**

9 We finally asked whether galvanotaxis of CNCCs is affected by the cell culture density.
10 Cell-cell contact has been shown to be important in chemotaxis of NCCs (Kasemeier-
11 Kulesa et al., 2006; Kasemeier-Kulesa et al., 2005; Krull et al., 1995; Theveneau et al.,
12 2010). The CNCCs migrate in three streams from the hindbrain, and cells within these
13 streams often form chainlike arrays, in which they maintain contact and migrate
14 collectively. CNCCs migrating together in chain have higher directionality than cells
15 migrating individually (Kulesa and Fraser, 1998; Teddy and Kulesa, 2004). Therefore, we
16 studied galvanotaxis in high density culture (approx. 620 cell/mm²), in which cells
17 maintained multiple cell-cell contact. **(Fig. 4, and Movie 7)**. Galvanotaxis of the cells in
18 high cell density cultures turned out to be very similar to that of low-density cultures
19 (approx. 150 cell/mm²) under the same strength of EF (15, 30, 50, 75, 100, and 200
20 mV/mm) **(Fig 4. A-F, H and Movie 7 vs. Fig 2. A-F, Fig 4. G, and Movie 4)**. The
21 directedness of high density CNCCs is slightly higher **(Fig 4. I)**, and displacement speed
22 is slightly lower **(Fig 4. J)** for every tested voltage strength but without statistical
23 significance.

1 **DISCUSSION**

2 Our results demonstrate that (1) mammalian CNCCs migrate towards the anode in
3 applied dcEFs of physiological strength; (2) Directedness, and displacement speed are
4 voltage-dependent with threshold likely to be between 15-30mV/mm, very similar to the
5 fields measured *in vivo* (27 ± 4 mV/mm) (Hotary and Robinson, 1994; Metcalf et al., 1994).

6 NCCs, arising over the vertebrate axis, start to emigrate from the midbrain region
7 in chick at approximately five to six somite stage (embryonic day (E) 1.5) (Tosney, 1982),
8 xenopus at stage 12 (Sadaghiani and Thiébaud, 1987), zebrafish at 13-14 hr
9 postfertilization (Schilling and Kimmel, 1994), and in mouse at five somite stage (E8.25)
10 (Nichols, 1986). The migration is critical for development and the underlying mechanisms
11 have been investigated, mostly for chemotaxis, and more recently for durotaxis (Barriga
12 et al., 2018; Dyson et al., 2018; Shellard and Mayor, 2019; Shellard et al., 2018; Szabo
13 and Mayor, 2018).

14 **Naturally occurring EFs in embryos and galvanotaxis of NCCs**

15 Endogenous EFs occur naturally in embryos. The activity of various ion pumps and
16 transporters generate charge difference across the epithelium that is manifested as
17 transepithelial potential (TEP) (Kennard and Theriot, 2020; Shi and Borgens, 1995). The
18 TEP across the embryonic ectoderm is the driving force capable of producing ionic-
19 current flow through, and out, of the embryos at the region of low electric resistance. This
20 current flow in turn sets up endogenous EFs within the embryos (Metcalf and Borgens,
21 1994; Metcalf et al., 1994). TEPs have been recorded during blastula, gastrula, and
22 neurula stages in amphibian, in primitive streak, during later stages development in the

1 chick, and have also been suggested in mouse blastomeres (Jaffe and Stern, 1979;
2 McCaig and Robinson, 1982; Metcalf et al., 1994; Nuccitelli, 1992; Nuccitelli and Wiley,
3 1985; Regen and Steinhardt, 1986). Modification of these fields during neurulation can
4 cause developmental abnormalities (Nuccitelli, 2003). It was suggested that EFs in the
5 range of 20-200 mV/mm exist along the migration pathways of NCCs.

6 Avian and amphibian NCCs in culture showed directional migration, even in an EF
7 as low as 7mV/mm (Nuccitelli et al., 1993). Our results add experimental evidence that
8 mammalian cranial NCCs also have robust galvanotaxis response. The threshold of EFs
9 to increase displacement speed and to induce directional migration appears to lie
10 between 15- 30 mV/mm (**Figs. 2, 3, 4**). These threshold values fall into the voltage
11 gradients detected in avian and amphibian embryos (Jaffe and Stern, 1979; McCaig and
12 Robinson, 1982; Metcalf et al., 1994; Nuccitelli, 1992; Nuccitelli and Wiley, 1985; Regen
13 and Steinhardt, 1986). Another interesting point is that the directedness values of
14 galvanotaxis in threshold fields seem fall in the range of average migration directionality
15 of NCC in vivo from (0.19 ± 0.1 to 0.3 ± 0.1) (Kulesa et al., 2004; Kulesa and Fraser,
16 1998) (Fig. 2G and Fig. 3H).

17 **Anode vs. cathode galvanotaxis of NCCs**

18 The avian and amphibian NCCs migrate toward the cathode (Cooper and Keller,
19 1984; Gruler and Nuccitelli, 1991). Mouse CNCCs, however, showed anodal
20 galvanotaxis, opposite to previous reported cathodal migration of avian and amphibian
21 NCCs. In the absence of EFs, CNCCs are flatter, have multipolar protrusions with no
22 preferential direction of cell protrusion and migration (**movie 1**). CNCCs in EFs assume

1 a morphology with long bipolar filipodia perpendicular to the field line, and smaller active
2 protrusions projected in the direction of migration (**Movie 2**). Cell membrane protrusions
3 in the direction of migration is consistent with that reported *in vitro* as well as *in vivo* (Dang
4 et al., 2013; Kennard and Theriot, 2020; Pollard and Cooper, 2009).

5 Why is there such a contrasting difference in galvanotaxis direction? We speculate
6 that the difference may be due to lineage difference (cranial vs trunk population),
7 developmental stage, and/or due to different species from which cells have been isolated.
8 CNCCs are a special group of NCCs that have osteogenesis potential (Le Douarin and
9 Kalcheim, 1999; Noden, 1988; Santagati and Rijli, 2003; Szabo and Mayor, 2018).
10 Osteogenesis were confirmed in both the O9-1 and primary cells (**Fig. 3 C**), confirming
11 this unique property. CNCCs also have very distinct gene expression profiles, different
12 from the trunk NCCs (Hu et al., 2014; Rothstein et al., 2018). It was suggested that axial-
13 specific genetic circuits operate in each subpopulation and underlie their unique features.
14 Such phylogenic difference may impact vertebrate evolution (Clay and Halloran, 2010;
15 Kuo and Erickson, 2011; Rothstein et al., 2018). NCCs used in previous studies were
16 more likely to be the trunk subpopulations from earlier stage of development. Species
17 difference might be a possible reason, because mammalian NCCs have some unique
18 features (Barriga et al., 2015; Simões-Costa and Bronner, 2015). Indeed, species
19 difference in NCC migration is recently been elegantly demonstrated with ray-finned
20 fishes (Stundl et al., 2020).

21 In conclusion, externally applied EFs with a threshold voltage between 15-
22 30mV/mm direct mammalian CNCCs to migrate towards the anode with increased
23 displacement speed. This threshold voltage is of the size reported in embryos.

1 Galvanotaxis alongside well-elucidated chemotaxis and durotaxis, is likely to regulate
2 NCC migration. Further investigation is warranted to determine galvanotaxis in guiding
3 migration of NCCs in development, especially the craniofacial development.

4

5

6 **Acknowledgment**

7 We thank Dr. Brian Reid for proofreading and editing the manuscript.

8 **Competing interests**

9 None

10

11 **Funding**

12 This work is supported by the AFOSR-MURI grant FA9550-16-1-0052, and NIH
13 1R01EY019101. This study was also supported by the NIH (grants R01AR066782,
14 R01AR068835, R01DE029353), UCLA/NIH CTSI (grant UL1TR000124). Work in Zhao
15 Laboratory is also supported by NEI Core Grant (P-30 EY012576, PI. Jack Werner / Marie
16 Burns) and a DARPA Award (HR001119S0027) (Lead PI Dr. Marco Rolandi, UC Santa
17 Cruz). We are also grateful to the following support: Louis and Karen Burns family
18 donation, Unrestricted Grant from Research to Prevent Blindness, Inc.

19

1 **References**

- 2 Abzhanov, A., Kuo, W.P., Hartmann, C., Grant, B.R., Grant, P.R., Tabin, C.J., 2006. The
3 calmodulin pathway and evolution of elongated beak morphology in Darwin's finches.
4 *Nature* 442, 563-567.
- 5 Allen, Greg M., Mogilner, A., Theriot, Julie A., 2013. Electrophoresis of Cellular Membrane
6 Components Creates the Directional Cue Guiding Keratocyte Galvanotaxis. *Current Biology*
7 23, 560-568.
- 8 Bajanca, F., Gougnard, N., Colle, C., Parsons, M., Mayor, R., Theveneau, E., 2019. In vivo
9 topology converts competition for cell-matrix adhesion into directional migration. *Nature*
10 *communications* 10, 1518-1518.
- 11 Baker, C.V.H., Bronner-Fraser, M., 1997. The origins of the neural crest. Part I: embryonic
12 induction. *Mech Dev* 69, 3-11.
- 13 Barlow, A.J., Dixon, J., Dixon, M.J., Trainor, P.A., 2012. Balancing neural crest cell intrinsic
14 processes with those of the microenvironment in Tcof1 haploinsufficient mice enables
15 complete enteric nervous system formation. *Hum Mol Genet* 21, 1782-1793.
- 16 Barriga, E.H., Franze, K., Charras, G., Mayor, R., 2018. Tissue stiffening coordinates
17 morphogenesis by triggering collective cell migration in vivo. *Nature* 554, 523-527.
- 18 Barriga, E.H., Trainor, P.A., Bronner, M., Mayor, R., 2015. Animal models for studying neural
19 crest development: is the mouse different? *Development (Cambridge, England)* 142,
20 1555-1560.
- 21 Chang, F., Minc, N., 2014. Electrochemical control of cell and tissue polarity. *Annu Rev Cell Dev*
22 *Biol* 30, 317-336.
- 23 Chen, X., Wang, H., Yu, M., Kim, J.K., Qi, H., Ha, P., Jiang, W., Chen, E., Luo, X., Needle, R.B., Baik,
24 L., Yang, C., Shi, J., Kwak, J.H., Ting, K., Zhang, X., Soo, C., 2019. Cumulative inactivation of
25 *Nell-1* in *Wnt1* expressing cell lineages results in craniofacial skeletal hypoplasia and
26 postnatal hydrocephalus. *Cell Death Differ*.
- 27 Chen, X., Wang, H., Yu, M., Kim, J.K., Qi, H., Ha, P., Jiang, W., Chen, E., Luo, X., Needle, R.B., Baik,
28 L., Yang, C., Shi, J., Kwak, J.H., Ting, K., Zhang, X., Soo, C., 2020. Cumulative inactivation of
29 *Nell-1* in *Wnt1* expressing cell lineages results in craniofacial skeletal hypoplasia and
30 postnatal hydrocephalus. *Cell Death & Differentiation* 27, 1415-1430.
- 31 Clay, M.R., Halloran, M.C., 2010. Control of neural crest cell behavior and migration: Insights
32 from live imaging. *Cell Adh Migr* 4, 586-594.
- 33 Cooper, M.S., Keller, R.E., 1984. Perpendicular orientation and directional migration of
34 amphibian neural crest cells in dc electrical fields. *Proc Natl Acad Sci U S A* 81, 160-164.
- 35 Cordero, D.R., Brugmann, S., Chu, Y., Bajpai, R., Jame, M., Helms, J.A., 2011. Cranial neural crest
36 cells on the move: their roles in craniofacial development. *Am J Med Genet A* 155A, 270-
37 279.
- 38 Crane, J.F., Trainor, P.A., 2006. Neural Crest Stem and Progenitor Cells. *Annual Review of Cell*
39 *and Developmental Biology* 22, 267-286.
- 40 Dang, I., Gorelik, R., Sousa-Blin, C., Derivery, E., Guérin, C., Linkner, J., Nemethova, M.,
41 Dumortier, J.G., Giger, F.A., Chipysheva, T.A., Ermilova, V.D., Vacher, S., Campanacci, V.,
42 Herrada, I., Planson, A.-G., Fetics, S., Henriot, V., David, V., Oguievetskaia, K., Lakisic, G.,
43 Pierre, F., Steffen, A., Boyreau, A., Peyriéras, N., Rottner, K., Zinn-Justin, S., Cherfils, J.,

1 Bièche, I., Alexandrova, A.Y., David, N.B., Small, J.V., Faix, J., Blanchoin, L., Gautreau, A.,
2 2013. Inhibitory signalling to the Arp2/3 complex steers cell migration. *Nature* 503, 281-
3 284.

4 Dyson, L., Holmes, A., Li, A., Kulesa, P.M., 2018. A chemotactic model of trunk neural crest cell
5 migration. *Genesis* 56, e23239.

6 Epperlein, H.-H., Selleck, M.A.J., Meulemans, D., McHedlishvili, L., Cerny, R., Sobkow, L.,
7 Bronner-Fraser, M., 2007. Migratory patterns and developmental potential of trunk neural
8 crest cells in the axolotl embryo. *Developmental Dynamics* 236, 389-403.

9 Forrester, J.V., Lois, N., Zhao, M., McCaig, C., 2007. The spark of life: the role of electric fields in
10 regulating cell behaviour using the eye as a model system. *Ophthalmic Res* 39, 4-16.

11 Gilbert, S.F., Bender, G., Betters, E., Yin, M., Cebra-Thomas, J.A., 2007. The contribution of
12 neural crest cells to the nuchal bone and plastron of the turtle shell. *Integrative and
13 Comparative Biology* 47, 401-408.

14 Golding, J.P., Trainor, P., Krumlauf, R., Gassmann, M., 2000. Defects in pathfinding by cranial
15 neural crest cells in mice lacking the neuregulin receptor ErbB4. *Nature Cell Biology* 2,
16 103-109.

17 Gov, N.S., 2007. Collective cell migration patterns: Follow the leader. *Proceedings of the
18 National Academy of Sciences* 104, 15970.

19 Gruler, H., Nuccitelli, R., 1991. Neural crest cell galvanotaxis: new data and a novel approach to
20 the analysis of both galvanotaxis and chemotaxis. *Cell motility and the cytoskeleton* 19,
21 121-133.

22 Hall, B.K., 2000. The neural crest as a fourth germ layer and vertebrates as quadroblastic not
23 triploblastic. *Evolution & Development* 2, 3-5.

24 Hotary, K.B., Robinson, K.R., 1994. Endogenous Electrical Currents and Voltage Gradients in
25 *Xenopus* Embryos and the Consequences of Their Disruption. *Developmental Biology* 166,
26 789-800.

27 Hu, N., Strobl-Mazzulla, P.H., Bronner, M.E., 2014. Epigenetic regulation in neural crest
28 development. *Dev Biol* 396, 159-168.

29 Ishii, M., Arias, A.C., Liu, L., Chen, Y.B., Bronner, M.E., Maxson, R.E., 2012. A stable cranial
30 neural crest cell line from mouse. *Stem Cells Dev* 21, 3069-3080.

31 Jaffe, L.F., Stern, C.D., 1979. Strong electrical currents leave the primitive streak of chick
32 embryos. *Science* 206, 569.

33 James, A.W., Shen, J., Zhang, X., Asatrian, G., Goyal, R., Kwak, J.H., Jiang, L., Bengs, B., Culiati,
34 C.T., Turner, A.S., Seim Iii, H.B., Wu, B.M., Lyons, K., Adams, J.S., Ting, K., Soo, C., 2015.
35 NELL-1 in the treatment of osteoporotic bone loss. *Nat Commun* 6, 7362.

36 Jiang, X., Iseki, S., Maxson, R.E., Sucov, H.M., Morriss-Kay, G.M., 2002. Tissue Origins and
37 Interactions in the Mammalian Skull Vault. *Developmental Biology* 241, 106-116.

38 Kasemeier-Kulesa, J.C., Bradley, R., Pasquale, E.B., Lefcort, F., Kulesa, P.M., 2006. Eph/ephrins
39 and N-cadherin coordinate to control the pattern of sympathetic ganglia. *Development*
40 133, 4839-4847.

41 Kasemeier-Kulesa, J.C., Kulesa, P.M., Lefcort, F., 2005. Imaging neural crest cell dynamics during
42 formation of dorsal root ganglia and sympathetic ganglia. *Development* 132, 235-245.

43 Kennard, A.S., Theriot, J.A., 2020. Osmolarity-independent electrical cues guide rapid response
44 to injury in zebrafish epidermis. *bioRxiv*, 2020.2008.2005.237792.

1 Krull, C.E., Collazo, A., Fraser, S.E., Bronner-Fraser, M., 1995. Segmental migration of trunk
2 neural crest: time-lapse analysis reveals a role for PNA-binding molecules. *Development*
3 121, 3733-3743.

4 Kulesa, P., Ellies, D.L., Trainor, P.A., 2004. Comparative analysis of neural crest cell death,
5 migration, and function during vertebrate embryogenesis. *Developmental Dynamics* 229,
6 14-29.

7 Kulesa, P.M., Fraser, S.E., 1998. Neural Crest Cell Dynamics Revealed by Time-Lapse Video
8 Microscopy of Whole Embryo Chick Explant Cultures. *Developmental Biology* 204, 327-
9 344.

10 Kuo, B.R., Erickson, C.A., 2011. Vagal neural crest cell migratory behavior: a transition between
11 the cranial and trunk crest. *Developmental dynamics : an official publication of the*
12 *American Association of Anatomists* 240, 2084-2100.

13 Le Douarin, N., Kalcheim, C., 1999. *The neural crest*, 2nd ed. Cambridge University Press,
14 Cambridge, UK ; New York, NY, USA.

15 Levin, M., Pezzulo, G., Finkelstein, J.M., 2017. Endogenous Bioelectric Signaling Networks:
16 Exploiting Voltage Gradients for Control of Growth and Form. *Annu Rev Biomed Eng* 19,
17 353-387.

18 Levin, M., Selberg, J., Rolandi, M., 2019. Endogenous Bioelectrics in Development, Cancer, and
19 Regeneration: Drugs and Bioelectronic Devices as Electroceuticals for Regenerative
20 Medicine. *iScience* 22, 519-533.

21 Litsiou, A., Hanson, S., Streit, A., 2005. A balance of FGF, BMP and WNT signalling positions the
22 future placode territory in the head. *Development* 132, 4051.

23 Marcucio, R.S., Cordero, D.R., Hu, D., Helms, J.A., 2005. Molecular interactions coordinating the
24 development of the forebrain and face. *Developmental Biology* 284, 48-61.

25 Mathews, J., Levin, M., 2018. The body electric 2.0: recent advances in developmental
26 bioelectricity for regenerative and synthetic bioengineering. *Current Opinion in*
27 *Biotechnology* 52, 134-144.

28 McCaig, C.D., Robinson, K.R., 1982. The ontogeny of the transepidermal potential difference in
29 frog embryos. *Developmental Biology* 90, 335-339.

30 Mehta, A.S., Luz-Madrigo, A., Li, J.-L., Tsonis, P.A., Singh, A., 2019. Comparative transcriptomic
31 analysis and structure prediction of novel *Newt* proteins. *PLoS one* 14, e0220416-
32 e0220416.

33 Mehta, A.S., Singh, A., 2017. Real time quantitative PCR to demonstrate gene expression in an
34 undergraduate lab. *Dros. Inf. Serv.* 100, 5.

35 Mehta, A.S., Singh, A., 2019. Insights into regeneration tool box: An animal model approach.
36 *Developmental Biology* 453, 111-129.

37 Metcalf, M.E.M., Borgens, R.B., 1994. Weak applied voltages interfere with amphibian
38 morphogenesis and pattern. *Journal of Experimental Zoology* 268, 323-338.

39 Metcalf, M.E.M., Shi, R., Borgens, R.B., 1994. Endogenous ionic currents and voltages in
40 amphibian embryos. *Journal of Experimental Zoology* 268, 307-322.

41 Minoux, M., Rijli, F.M., 2010. Molecular mechanisms of cranial neural crest cell migration and
42 patterning in craniofacial development. *Development* 137, 2605.

43 Nichols, D.H., 1986. Formation and distribution of neural crest mesenchyme to the first
44 pharyngeal arch region of the mouse embryo. *American Journal of Anatomy* 176, 221-231.

1 Noden, D.M., 1988. Interactions and fates of avian craniofacial mesenchyme. *Development* 103
2 Suppl, 121-140.

3 Nuccitelli, R., 1992. Endogenous ionic currents and DC electric fields in multicellular animal
4 tissues. *Bioelectromagnetics* 13, 147-157.

5 Nuccitelli, R., 2003. Endogenous electric fields in embryos during development, regeneration
6 and wound healing. *Radiation Protection Dosimetry* 106, 375-383.

7 Nuccitelli, R., Smart, T., 1989. Extracellular Calcium Levels Strongly Influence Neural Crest Cell
8 Galvanotaxis. *The Biological Bulletin* 176, 130-135.

9 Nuccitelli, R., Smart, T., Ferguson, J., 1993. Protein kinases are required for embryonic neural
10 crest cell galvanotaxis. *Cell Motility* 24, 54-66.

11 Nuccitelli, R., Wiley, L.M., 1985. Polarity of isolated blastomeres from mouse morulae:
12 Detection of transcellular ion currents. *Developmental Biology* 109, 452-463.

13 Pollard, T.D., Cooper, J.A., 2009. Actin, a Central Player in Cell Shape and Movement. *Science*
14 326, 1208.

15 Regen, C.M., Steinhardt, R.A., 1986. Global properties of the *Xenopus* blastula are mediated by
16 a high-resistance epithelial seal. *Developmental Biology* 113, 147-154.

17 Reyes, M., Zandberg, K., Desmawati, I., de Bellard, M.E., 2010. Emergence and migration of
18 trunk neural crest cells in a snake, the California Kingsnake (*Lampropeltis getula*
19 *californiae*). *BMC Dev Biol* 10, 52-52.

20 Rothstein, M., Bhattacharya, D., Simoes-Costa, M., 2018. The molecular basis of neural crest
21 axial identity. *Dev Biol* 444 Suppl 1, S170-S180.

22 Ruhrberg, C., Schwarz, Q., 2010. In the beginning: Generating neural crest cell diversity. *Cell*
23 *Adh Migr* 4, 622-630.

24 Sadaghiani, B., Thiébaud, C.H., 1987. Neural crest development in the *Xenopus laevis* embryo,
25 studied by interspecific transplantation and scanning electron microscopy. *Developmental*
26 *Biology* 124, 91-110.

27 Santagati, F., Rijli, F.M., 2003. Cranial neural crest and the building of the vertebrate head. *Nat*
28 *Rev Neurosci* 4, 806-818.

29 Schilling, T.F., Kimmel, C.B., 1994. Segment and cell type lineage restrictions during pharyngeal
30 arch development in the zebrafish embryo. *Development* 120, 483.

31 Shellard, A., Mayor, R., 2019. Integrating chemical and mechanical signals in neural crest cell
32 migration. *Current opinion in genetics & development* 57, 16-24.

33 Shellard, A., Szabo, A., Trepap, X., Mayor, R., 2018. Supracellular contraction at the rear of
34 neural crest cell groups drives collective chemotaxis. *Science* 362, 339-343.

35 Shi, R., Borgens, R.B., 1995. Three-dimensional gradients of voltage during development of the
36 nervous system as invisible coordinates for the establishment of embryonic pattern.
37 *Developmental Dynamics* 202, 101-114.

38 Simões-Costa, M., Bronner, M.E., 2015. Establishing neural crest identity: a gene regulatory
39 recipe. *Development (Cambridge, England)* 142, 242-257.

40 Song, B., Gu, Y., Pu, J., Reid, B., Zhao, Z., Zhao, M., 2007. Application of direct current electric
41 fields to cells and tissues in vitro and modulation of wound electric field in vivo. *Nature*
42 *Protocols* 2, 1479-1489.

1 Stundl, J., Pospisilova, A., Matejkova, T., Psenicka, M., Bronner, M.E., Cerny, R., 2020. Migratory
2 patterns and evolutionary plasticity of cranial neural crest cells in ray-finned fishes. *Dev*
3 *Biol.*

4 Szabo, A., Mayor, R., 2018. Mechanisms of Neural Crest Migration. *Annu Rev Genet* 52, 43-63.

5 Szabó, A., Theveneau, E., Turan, M., Mayor, R., 2019. Neural crest streaming as an emergent
6 property of tissue interactions during morphogenesis. *PLoS Comput Biol* 15, e1007002-
7 e1007002.

8 Teddy, J.M., Kulesa, P.M., 2004. In vivo evidence for short- and long-range cell communication
9 in cranial neural crest cells. *Development* 131, 6141-6151.

10 Theveneau, E., Marchant, L., Kuriyama, S., Gull, M., Moepps, B., Parsons, M., Mayor, R., 2010.
11 Collective chemotaxis requires contact-dependent cell polarity. *Developmental cell* 19, 39-
12 53.

13 Tosney, K.W., 1982. The segregation and early migration of cranial neural crest cells in the avian
14 embryo. *Developmental Biology* 89, 13-24.

15 Trainor, P.A., 2005. Specification of neural crest cell formation and migration in mouse
16 embryos. *Semin Cell Dev Biol* 16, 683-693.

17 Trainor, P.A., 2010. Craniofacial birth defects: The role of neural crest cells in the etiology and
18 pathogenesis of Treacher Collins syndrome and the potential for prevention. *Am J Med*
19 *Genet A* 152A, 2984-2994.

20 Trainor, P.A., Sobieszczuk, D., Wilkinson, D., Krumlauf, R., 2002. Signalling between the
21 hindbrain and paraxial tissues dictates neural crest migration pathways. *Development*
22 129, 433.

23 Walheim, C.C., Zanin, J.P., de Bellard, M.E., 2012. Analysis of trunk neural crest cell migration
24 using a modified Zigmond chamber assay. *J Vis Exp*, 3330.

25 Walker, M.B., Trainor, P.A., 2006. Craniofacial malformations: intrinsic vs extrinsic neural crest
26 cell defects in Treacher Collins and 22q11 deletion syndromes. *Clinical Genetics* 69, 471-
27 479.

28 Wong, G.L., Cohn, D.V., 1975. Target cells in bone for parathormone and calcitonin are
29 different: enrichment for each cell type by sequential digestion of mouse calvaria and
30 selective adhesion to polymeric surfaces. *Proc Natl Acad Sci U S A* 72, 3167-3171.

31 Wynn, M.L., Rupp, P., Trainor, P.A., Schnell, S., Kulesa, P.M., 2013. Follow-the-leader cell
32 migration requires biased cell-cell contact and local microenvironmental signals. *Phys Biol*
33 10, 035003-035003.

34 Zhang, X., Kuroda, S., Carpenter, D., Nishimura, I., Soo, C., Moats, R., Iida, K., Wisner, E., Hu,
35 F.Y., Miao, S., Beanes, S., Dang, C., Vastardis, H., Longaker, M., Tanizawa, K., Kanayama,
36 N., Saito, N., Ting, K., 2002. Craniosynostosis in transgenic mice overexpressing *Nell-1*. *J*
37 *Clin Invest* 110, 861-870.

38 Zhao, S., Mehta, A.S., Zhao, M., 2020. Biomedical applications of electrical stimulation. *Cellular*
39 *and Molecular Life Sciences.*

40

1 **Figure Legends**

2 **Fig 1. Galvanotaxis of mammalian cranial neural crest cell (CNCC) line – ‘O9-1’.**
3 **(A,B)** Migration of CNCCs in control cultures without applying EF **(C,D)** Significant
4 directional migration of CNCC to the anode in an applied EF. B and D show the migration
5 tracks of CNCCs for 3 hours as in A and C respectively. **(E,F,G)** Reversal of EF polarity
6 reversed cell migration direction. **(F)** In the first 2 hours cells move toward the anode on
7 the left. Then the field polarity was reversed for next 2 hours. **(G)** Cells reversed their
8 direction within 5-10 minutes following reversal of field polarity and migrated towards the
9 new anode on the right. Migration trajectories of selected cells in A, C and E are presented
10 as temporal color codes. F and G show migration tracks as from E for total of 4 hrs with
11 field polarity reversed after 2 hrs. Cells migrate towards the left are shown in red, and to
12 the right in black. The position of all cells in B,D, F, G, at t = 0 min is positioned at the
13 origin (0, 0). n= 50 cells from one experiment and confirmed in two additional experiments.
14 O9-1 cells were cultured in complete ES cell medium with 15% FBS and LIF + 25 ng/ml
15 recombinant human bFGF. EF= 200 mV/mm.

16 **Fig 2. Voltage dependence of galvanotaxis of mammalian CNCC (O9-1 cell line). (A-**
17 **F).** Migration trajectories of CNCCs for 3 hrs. All cells started from the origin. Cells
18 migration towards the anode to the left are shown in red, and towards the cathode to the
19 right in black **(G)**. The migration directedness, and **(H)** displacement speed of CNCCs
20 increase with the increasing field strength. Data are mean \pm SEM. *P<0.05, **P<0.01,
21 ***P<0.001.

22 **Fig 3. Galvanotaxis of primary CNCCs. (A)** Primary CNCCs were isolated from the
23 frontal and nasal bones of neonatal mouse cranial vault (green part labeled). They were
24 expanded in growth medium (passages 3-5). Cranial lineage of primary culture of CNCCs
25 were validated by **(B)** RT-qPCR and **(C)** Osteogenic differentiation. **(B)** Gene expression
26 of NCC markers (*Snail1*, *Twist1*, *Nestin*, *CD44* and *Sca-1*) in primary NCCs was
27 normalized to O9-1 CNCCs. N=3, each template underwent reverse transcription from an
28 RNA pool of 3 experimental sets of cells. **(C)** Osteogenic differentiation of O9-1 and
29 primary CNCCs were initiated by culturing the cells in osteogenic differentiation medium
30 (ODM) (+/- 100ng/ml BMP2). ALP staining was performed on Day-7, and AR staining was
31 performed on Day-21. Images are representative from triplicates of each group. **(D-G)**
32 Migration trajectories. Cells migrate towards the anode to the left as shown in red, and
33 towards cathode to the right in black. All cells started from the origin and migrated for 3
34 hours. **(H)** Applied EFs directed cell migration **(I)** increased displacement speed. *P<0.05,
35 **P<0.01, *** P<0.001 when compared to the no EF control. Scale bar 50 μ m.

36 **Fig 4. CNCCs in high density cultures showed similar galvanotaxis. (A-F)** Cell
37 migration trajectories in high density culture, with starting position from the origin for 3
38 hours. All cells started from the origin. Cells migration towards the anode to the left are
39 shown in red, and towards the cathode to the right in black. 50 CNCCs from one
40 experiment, repeated with two more experiments. Representative example of **(G)** low
41 density CNCCs and **(H)** high density CNCCs. **(I)** Migration directedness, and **(J)**

1 displacement speed of cells in high density cultures are very similar to that of cells in low
2 density culture in fields of all strengths tested.

3

4 **Movie Legends**

5 **Movie 1:** CNCCs (O9-1) migrate in random direction in no EF control culture.

6 **Movie 2:** CNCCs (O9-1) migrate directionally towards the anode to the left in an electric
7 field.

8 **Movie 3:** Reversal of EF polarity reverses migration direction of CNCCs from old anode
9 towards left (first 2hrs) to new anode towards right (another 2hrs).

10 **Movie 4:** Voltage dependent response of low density CNCCs (O9-1) in EFs of 15, 30, 50,
11 100, and 200 mV/mm. Anode on the left, and Cathode on the right.

12 **Movie 5:** Primary CNCCs migrate in random direction in no EF control culture.

13 **Movie 6:** Voltage dependent response of Primary CNCCs in EFs of 15, 100, and 200
14 mV/mm. Anode on the left, and Cathode on the right.

15 **Movie 7:** Voltage dependent response of high density CNCCs (O9-1) in EFs of 15, 30,
16 50, 100, and 200 mV/mm. Anode on the left, and Cathode on the right.

17

18

Figure 1.

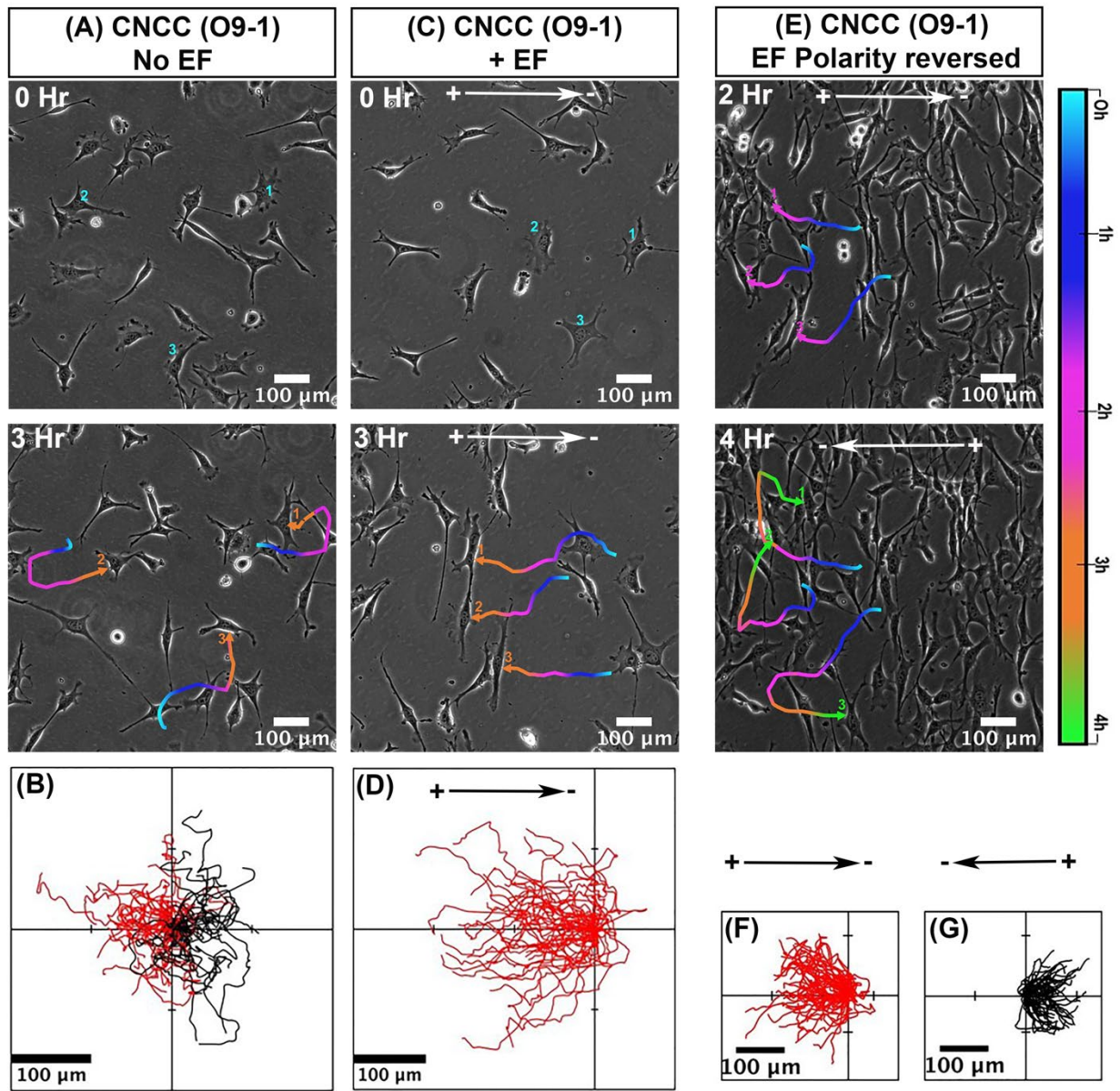
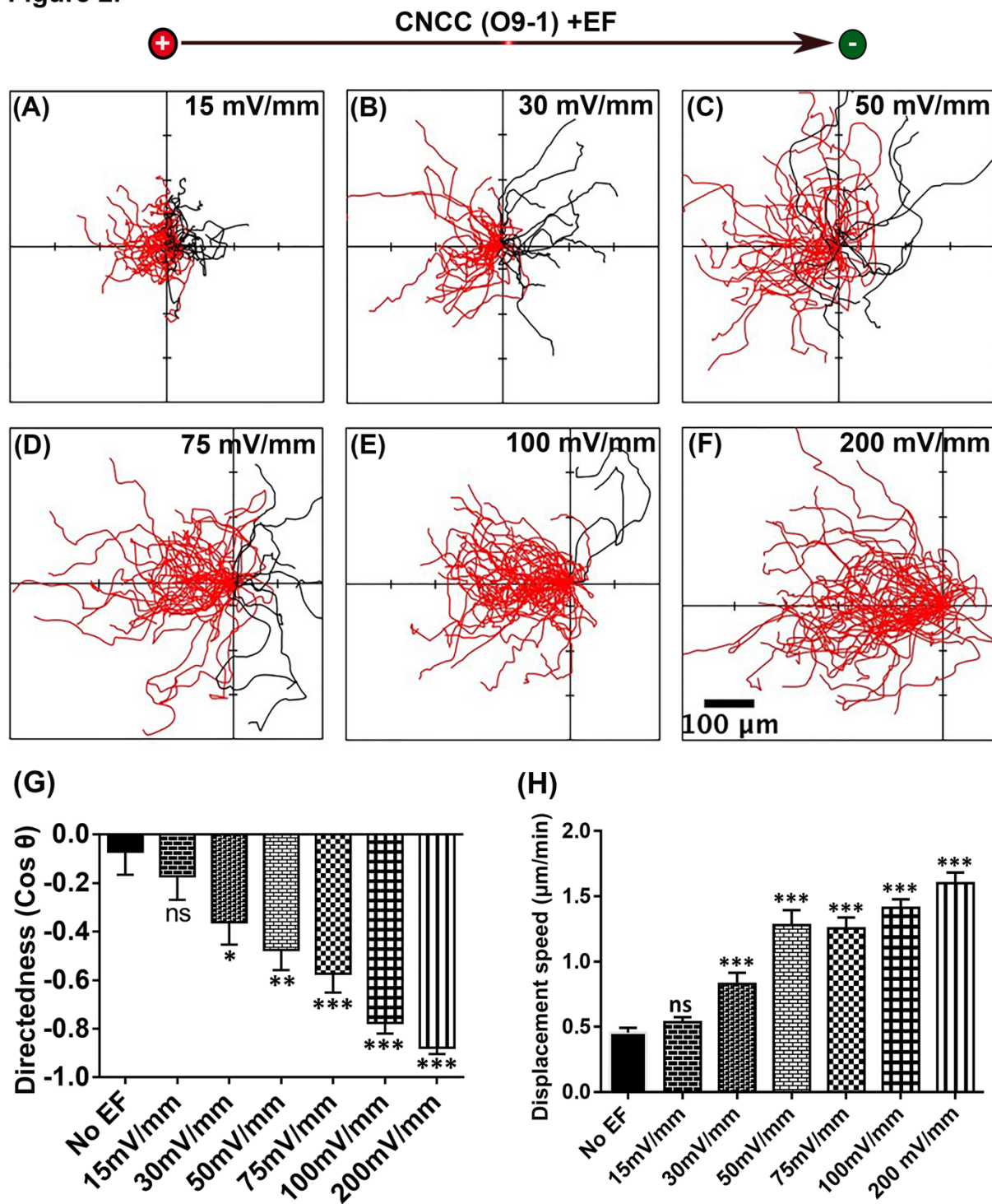


Figure 2.



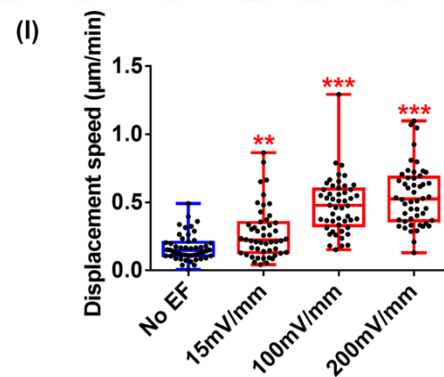
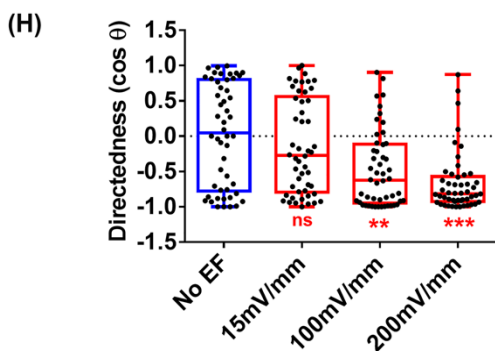
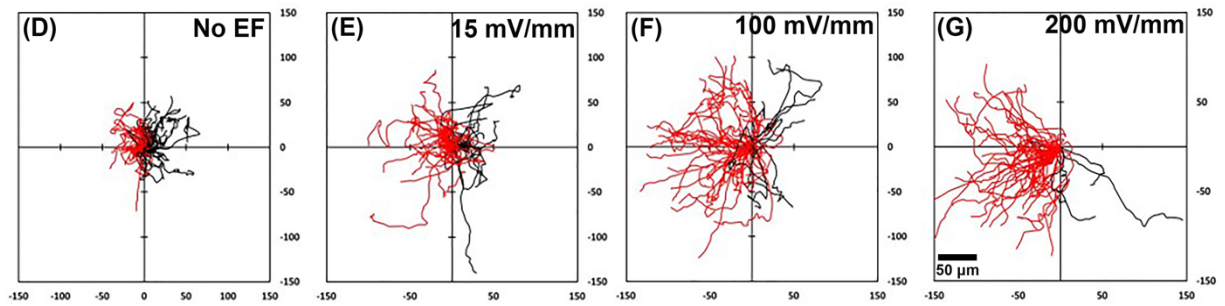
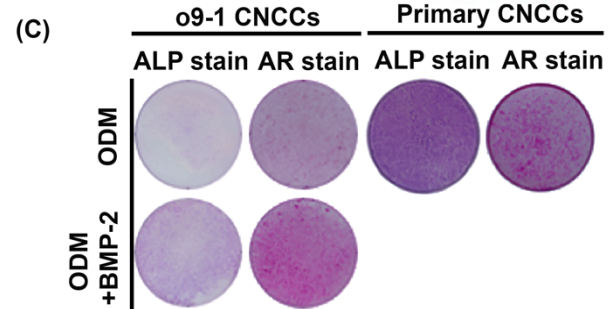
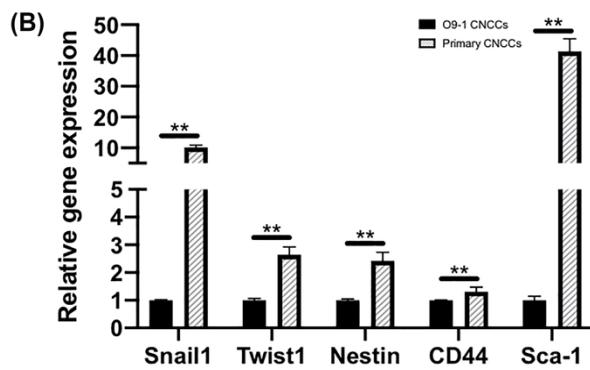
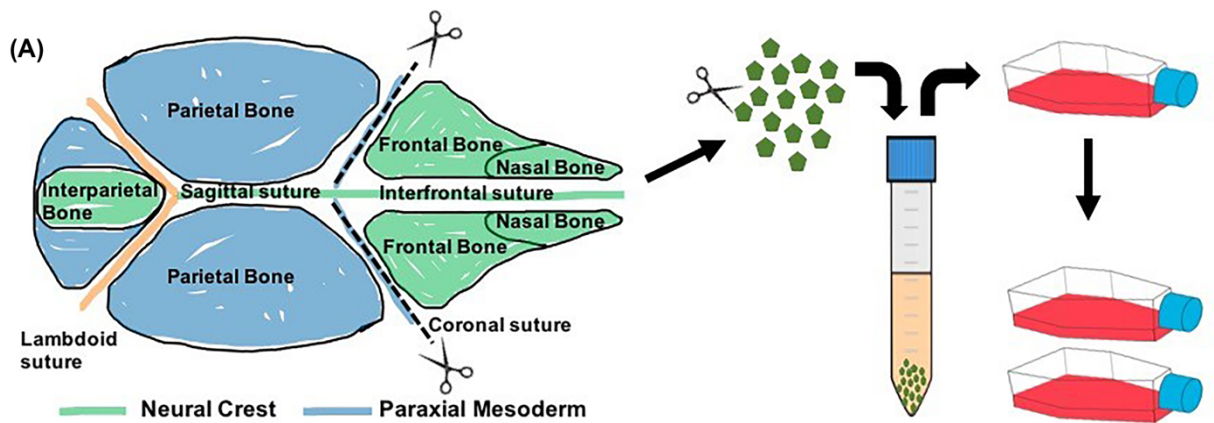


Figure 4.

